IEEE Access
Multidisciplinary ⋮ Rapid Review ⋮ Open Access Journal

Received March 21, 2022, accepted April 18, 2022, date of publication April 25, 2022, date of current version May 4, 2022.

Digital Object Identifier 10.1109/ACCESS.2022.3170453

nOMP: A New Sparse Solution to Enhance the SSIM Levels of OMP-Based Encoded Images

A. N. OMARA[1], HESHAM FAROUK[1], AND SAYED A. MOHAMED[2]
[1]Electronics Research Institute (ERI), El-Nozha, Cairo 11843, Egypt
[2]National Authority for Remote Sensing and Space Sciences (NARSS), El-Nozha, Cairo 11843, Egypt

Corresponding author: A. N. Omara (ahmed_omara@eri.sci.eg)

This work was supported by the Egyptian Academy of Scientific Research and Technology (ASRT) under Project (Child Tut).

ABSTRACT This work comprises the development of a quality enhancement technique for image encoders that use compressive sensing. The recommended solution seeks to maximize the perceptual quality based objective function, unlike other sparse representation algorithms that minimizes the error-based objective function. The key idea behind this work is to develop an iterative methodology that works as a modifier for the sparse coefficients. The modification procedure is SSIM-based and has been carried out in an iterative and linear manner. The conducted experiments revealed that the recommended technique works better than another SSIM-based modifier termed the SSIM-inspired OMP (iOMP) in terms of SSIM levels gained. The t-test is also utilized to examine our performance for significance, and the results show that the method works well for any type of image and any size, especially when a data-independent based dictionary is used.

INDEX TERMS Orthogonal matching pursuit, compressive sensing, structural similarity index, image enhancement.

I. INTRODUCTION

Nowadays, the image signal could be considered one of the most important signals. But, images become prone to manifestation of some random noise during image acquisition or restoration processes. The main source of image's noise is the acquisition process, and it occurs due to the inherent physical limitations of various recording devices such as the pixel size which depends mainly on the steady progress of the semiconductor technology. Beside this type of inherent noise, the image is usually processed to extract some information and this processing may distort the image progressively. Recently, there is a need to represent the image sparsely, and this type of representations is a lossy technique. So, after image acquisition, the image is exposed to another type of noise which is processing-based noise.

One of the main issues of current image denoisers is that, they usually use the mean squared error (MSE) as the main image fidelity metric. But, many researches proved that the MSE suffers from many drawbacks when it is used as a quality metric for the images. In [1], the results of an assessment in connection with the usefulness of a number of objective quality measurements for grayscale image compression had been offered. It was evident that although a group of numerical measures can surely be used to assign the amount of degradation in reconstructed images for a given compression technique, an assessment across different techniques is not possible. This is because a single scalar value cannot be used to depict a diversity of impairments. In [2], the authors listed the drawbacks of the MSE-based metrics such as peak signal to noise ratio (PSNR), root mean squared error (RMSE), mean absolute error (MAE), and signal to noise ratio (SNR) which have been used as image quality measurement for a long time. MSE-based metrics do not take into account image dependencies such as textures, orderings, patterns, etc. all of which affect image perception quality. Image pixel order transmit vital information about the structure of a visual scene. Unfortunately the MSE-based metrics do not measure this. The correlation between the error signal and the underlying image affects significantly on the perceptual image distortion but this is also ignored by the MSE-based metrics. Also, they do not take into account the signs of the error (since its square is used) signal added to an image. However, the visual fidelity of the resulting image has been proved to be drastically different. Since all

The associate editor coordinating the review of this manuscript and approving it for publication was Yongjie Li.

images are treated equally in the formulation of the MSE, image content dependent variations in image fidelity cannot be accounted for.

Besides the MSE-based metrics, there is another class of measurement methods which consider the human visual system (HVS) characteristics in an attempt to incorporate perceptual quality measures [3]. But the HVS-based metrics are complicated and have not any clear advantages over the MSE-based methods under strict testing conditions and different image distortion environments [4]. Later, Zhou Wang and Alan C. Bovik proposed a Universal Quality Index (UQI) titled "Structural Similarity Index (SSIM)" in [4]. The suggested index is designed by modeling any image distortion as a combination of three factors: contrast distortion, luminance distortion, and loss of correlation. Although the SSIM is described mathematically and no human visual system model is explicitly employed, the conducted experiments on various image distortion types indicate that it performs significantly better than the MSE-based metrics.

For the image distortions which are caused by the sparse representation, we propose a new quality enhancement technique that considers into account the SSIM as the main image fidelity metric. All contributions of this paper can be summarized as follows:

- Present a novel sparse solution called "Near-OMP" or shortly "nOMP," which is based on SSIM as the main fidelity metric rather than the MSE.
- Studying the computational complexity of the proposed algorithm.
- For validating the effectiveness of the new sparse solution, we use many images belonging to variant datasets. In addition, a comparison among different denoising methods has been conducted.
- Another hybrid methods have been proposed and evaluated.

Therefore, the rest of this paper is organized as follows. A detailed literature review is presented in Section II. The proposed approach is illustrated in a detailed manner in Section III, the numerical simulation study is presented in Section IV. Finally, the conclusions are presented in section V.

II. BACKGROUND

Numerous denoising techniques for images have been proposed in various works. As illustrated in [5], on the basis of the type of denoising algorithms, they can broadly be referred to as: spatial domain filtering, transform domain thresholding, random fields, statistical models, anisotropic diffusion methods, sparse modeling, dictionary learning methods and hybrid methods [6]. Besides these methods, there are some major denoising measures include spatial adaptive filters, statistical estimators of all sorts, stochastic analysis, morphological analysis and order statistics [7].

Before going over the sparse modeling-based image denoisers, it's important to take a look at the greedy pursuit algorithms, which are at the heart of sparse modeling.

A. GREEDY PURSUIT ALGORITHMS

It was first introduced in [8] and [9] as a method to find sparse linear combinations of basis functions to encode natural images. Sparse representation of signals is a growing field of research which aims at finding a set of prototype signals called atoms $\varphi \in \mathbb{R}^M$ which forms a dictionary $\Phi \in \mathbb{R}^{M\times N}$ that can be used to represent a particular set of a given signal $x \in \mathbb{R}^M$ by some sparse linear combination of the atoms in the dictionary. Mathematically, for the given signal, we need to find the suitable atoms in Φ such that

$$x = \Phi C^{(k)} + e \tag{1}$$

where $C^{(k)}$ is a k-sparse vector which contains k non-zero weights for the linear combination, and e is the reconstruction error vector. $C^{(k)}$ could be obtained iteratively by solving the l_0-norm minimization problem,

$$C^{(k)} = \underset{C}{argmin}\ \|x - \Phi C\|_2^2 + \lambda \|C\|_0 \tag{2}$$

Commonly used strategies for solving the (l_0) sparse optimization problem are called greedy pursuit algorithms, the most important of which are Matching Pursuit (MP) [10], Orthogonal Matching Pursuit (OMP) [11], and Orthogonal Least Squares (OLS) [12]. OMP typically shows greatly superior performance to MP, however, OMP is more costly in both computation time and storage requirements. As shown in Equation 2, the term $\|x-\Phi C\|_2^2$ is simply the squared error, and it is not a quality indicator like the SSIM for images as discussed in [13].

In addition to Equation 2, there are different objective functions in which the term $\|C\|_0$ is replaced with $\|C\|_1$, or $\|C\|_p$, where $0 < p < 1$. The Lasso problem [14] gave rise to the l_1-norm, which has been widely applied to problems in machine learning, pattern recognition, and statistics [15]–[17]. Recent literature [18]–[21] has shown that when the representation solution obtained using the l_1-norm minimization constraint satisfies the condition of sparsity, the solution obtained using l_1-norm minimization with sufficient sparsity can be equivalent to the solution obtained using l_0-norm minimization with full probability.

In addition to the l_0-norm minimization and l_1-norm minimization, several authors are trying to handle the sparse representation problem with the l_p-norm minimization, especially $p = 0.1, \frac{1}{2}, \frac{1}{3}$, or 0.9 [22]–[24]. Despite the fact that l_p-norm minimization sparse representation methods are not the most used approaches for obtaining a sparse representation solution, they have a significant impact on the sparse representation theory.

B. SPARSE MODELING-BASED IMAGE DENOISERS

In this section, we will focus on those works that exploits the sparse representation to make image denoising. These works may be classified into two categories. The first category includes all methods that use the sparse modeling as a denoising tool, i.e., the image is already corrupted by a source of noise and would be denoised by a sparse modeling

technique. As for the second category, it includes all methods that make denoising for all images corrupted by a sparse modeling technique.

In 2006, Elad introduced a paper entitled ''Image Denoising Via Sparse and Redundant Representations Over Learned Dictionaries'' [25]. In this work, a simple method has been presented to denoise any image which is corrupted by a white Gaussian noise with zero-mean. The proposed method is based on local operations and involves sparse decompositions of each image block under one fixed overcomplete dictionary, and a simple average calculations. The content of the dictionary is of prime importance for the denoising process. Under the same category, in 2007, Kostadin introduced a paper entitled ''Image Denoising by Sparse 3-D Transform-Domain Collaborative Filtering'' [26]. In this work, the similar image block or patches are grouped using cluster techniques, then, the 2D blocks are stacked together forming a 3D array. Furthermore, a collaborative Wiener filtering is applied on the obtained 3D arrays. This work can be adapted to various noise models such as additive colored noise, non-Gaussian noise, etc., by modifying the calculation of coefficients' variances in the basic and Wiener parts of the algorithm. In addition, the developed method can be modified for denoising 1-D-signals and video, for image restoration, as well as for other problems that can benefit from highly sparse signal representations.

In 2008, Julien Mairal introduced a research entitled ''Sparse Representation for Color Image Restoration'' [27]. The goal of this work is to extend the algorithm reported in [25] to the vector-valued images, and then show the applicability of this extension to other inverse problems in color image processing. The extension to color can be easily performed by a simple concatenation of the RGB values to a single vector and training on those directly, which gives already better results than denoising each channel separately. However, such a process produces false colors and artifacts, which are typically encountered in color image processing.

Another work was introduced in 2009 by Priyam and entitled ''Clustering-Based Denoising With Locally Learned Dictionaries'' [28]. This work belongs to a class between methods that can be categorized as kernel regression based, and those that aim to learn the best global dictionary. In this work, the denoising process passess through three stages: clustering stage where the image is clustered using features that capture the local structure of the underlying image data (patches of pixels from the image), the dictionary selection stage where we form an optimized dictionary that adapts to the geometric structure of the image patches in each cluster; and, finally, the coefficient calculation stage where the coefficients for the linear combination of dictionary atoms are estimated, subject to the (steering) kernel weights.

All methods mentioned in this section are MSE-based. But, later in 2012, Abdul Rehman and Rostami introduced a work entitled ''SSIM inspired image restoration using sparse representation'' [29]. Up to our knowledge, this work could be considered the first one that takes into account the SSIM as a modifier to the sparse coefficients. So, next section makes a detailed review on this work, because it will be compared later by our proposed algorithms.

C. SSIM INSPIRED OMP DENOISER (IOMP)

Unlike OMP, the iOMP methodology suggested by [29] has another objective function:

$$\{C, \hat{x}\} = \underset{w}{argmin} \|C\|_0 \text{ subject to } \mathcal{SI}(x, \Phi C) \tag{3}$$

where $\mathcal{SI}(x, \Phi C)$ is the similarity index level between the original image x and the distorted image $\hat{x} = \Phi C$. Note that, as specified by iOMP, the function $\mathcal{SI}(x, \Phi C)$ is not only a computation for the similarity index level, but also, there is a try to get the best value for SSIM per iteration.

$$\mathcal{SI}(x, \hat{x}) = \frac{2\mu_x\mu_{\hat{x}} + F_1}{{\mu_x}^2 + {\mu_{\hat{x}}}^2 + F_1} \frac{2\sigma_{x\hat{x}} + F_2}{{\sigma_x}^2 + {\sigma_{\hat{x}}}^2 + F_2} \tag{4}$$

Both OMP and iOMP are iterative in nature, and at first iteration, both find the dc component of the representation process $x_{dc} = \varphi_{dc} c_0$, where φ_{dc} is the normalized dc atom such that $\varphi_{dc} = \frac{1}{\sqrt{m}} \mathbb{1}$, and $\mathbb{1}$ is the ones vector. After acquiring this component, iOMP uses the same rules of OMP to get the next set of atoms and its optimal coefficients in $\mathcal{L}_2$ sense. But, henceforth, each iteration has a further step to get the optimal coefficients in SSIM sense. Mathematically, the authors in [29] proved that, the optimal coefficients in SSIM sense are directly proportional to that of $\mathcal{L}_2$ sense and the proportionality constant is β such that $\acute{C} = \beta C$, where $\acute{C}$ and C are the vector of iOMP's and OMP's ac coefficients. At each iteration, the proportionality constant could be calculated as follows:

$$\beta = \frac{-F_2 + \sqrt{F_2^2 + 4(B - A)(\sigma_x^2 + F_2)}}{2(B - A)} \tag{5}$$

where

$$A = \frac{1}{n-1} \sum_{i=1}^{k} \sum_{j=1}^{k} c_i c_j \langle \varphi_i, \varphi_j \rangle \tag{6}$$

$$B = \frac{2}{n-1} \sum_{j=1}^{k} c_j \langle x, \varphi_j \rangle \tag{7}$$

According to previous formulas, it could be said that β is constant for a given set of atoms. But, it should be recalculated if this set is updated.

In a later work [30], we discussed all issues of iOMP. In summary, our comments on iOMP are that, iOMP depends on the MSE-based OMP to select the suitable atoms from a dictionary. So, it is not pure SSIM-based technique. In addition, as stated before, β is computed to maximize the SSIM level. But, as done in [29], Equation 4 is differentiated one time to get β that maximizes SSIM level. But, this condition is not sufficient. Besides that, iOMP doesn't compare itself with the classical OMP after each iteration,

hence, there is no guarantee to enhance the SSIM levels which are obtained by OMP after each iteration.

III. NEAR-OMP APPROACH

As known, the ac coefficients carry energy depending on the amount of detail in the image block. However, most of the energy is compacted in the dc coefficient and a few ac coefficients. The main idea behind the proposed methodology which is titled "Near-OMP" or shortly "nOMP" is to find the best **ac** coefficients that maximizes the SSIM value regardless of the expected increase in the error level. The new ac coefficients vector C_n could be related to the OMP's ac coefficients C_o as follows:

$$C_n = \vec{\alpha} \odot C_o \tag{8}$$

where $\odot$ is the element-wise multiplication process, and $\vec{\alpha}$ is a vector of $k-1$ unknowns. To process of computing the $k-1$ unknowns of $\vec{\alpha}$ is an NP hard problem. For simplification, this study assumes that both vectors C_n and C_o are exactly in the same direction. So, Equation 8 could be simplified to:

$$C_n = \alpha C_o \tag{9}$$

where α is a constant. Now, the essential idea behind this approach is to find α that minimizes the following objective function:

$$f = 1 - SI\left(X, \sum_{i=1}^{k} \alpha c_i \varphi_i\right) \tag{10}$$

α is assumed to be near 1, and this assumption guarantees two main aspects. The first aspect is the least computational complexity and the other is to avoid the huge additive noise.

Assume X_o and X_n are the sparse approximation of a 8 image block by OMP and nOMP respectively. Then, these approximation could be written as follows:

$$X_o = X_{dc} + \Phi^T C_o \tag{11}$$
$$X_n = X_{dc} + \Phi^T C_n \tag{12}$$

The obtained error $\|X_n - X_o\|_2^2$ could be written as follows:

$$\|X_n - X_o\|_2^2 = \|\Phi^T (C_n - C_o)\|_2^2 \tag{13}$$
$$= \|\Phi^T C_o\|_2^2 (\alpha - 1)^2 \tag{14}$$

As shown, the quantity $(\alpha - 1)^2$ could be considered the normalized error e_{nor}. By putting a threshold level for $e_{nor} = e_{th}$, we can limit the iteration process of α that would be maximized by $\sqrt{e_{th}} + 1$.

First of all, at the sparseness level s of OMP, it updates its index set I by selecting the atom's index which maximizes the absolute value of $\varphi^T r_{omp}^{s-1}, \forall \varphi \in \Phi$ where r_{omp}^{s-1} is the last residual vector. Then, the ac coefficients C_o could be obtained by $\left(\Phi_I^T \Phi_I\right)^{-1} \Phi_I^T \mathbf{x}$. Now, we have $s-1$ ac coefficients that minimize the error $\|X - X_o|_2^2$. According to the literature review section, this minimization doesn't mean the maximal point of SSIM. So, nOMP starts from C_o to find another co-directed vector C_n, see Equation 9. The accepted values of C_n are the values that maximize the SSIM level. The new coefficient α is updated in iterative manner with a predefined step $\Delta\alpha$. For each new value of α, the SSIM is always checked to investigate whether or not the SSIM increases or not. The nOMP's iterations continue till the nearest maximum point of SSIM is reached.

A. METHODOLOGY

In detail, the nOMP methodology is illustrated in Figure 1. As shown, OMP works to minimize the L_2 by selecting the best **s** atoms from the dictionary Φ, then the obtained coefficients vector $C_o \in \mathbb{R}^s$ enters the nOMP's cycle to find the new coefficients C_n that maximizes the SSIM level at the sparseness level s. Like iOMP [29], the new coefficients are linearly dependent to the old coefficients. On the other side, it could be shown that, nOMP differs from iOMP as it doesn't take the new coefficients as a new starting point to the next iterations of OMP. So, it could be said that each iteration is a standalone. The overall algorithm finishes its task if the required SSIM level is reached. But, if the SSIM level is not reached, then the algorithm is halted if the sparseness level reached a predefined level **k**. Also, another difference between iOMP and nOMP exists. As illustrated in [29], iOMP finds the new coefficients in terms of the differentiation of the SSIM function, but this step is not sufficient to get the maximum point of structural index. So, nOMP avoids this issue by solving the optimization problem iteratively.

B. COMPLEXITY ANALYSIS

This section discusses the time complexity of nOMP algorithm. First of all, this analysis is performed on one image block, so, the overall complexity will be as order of the number of blocks.

To analyze the nOMP's complexity, let us decompose it to separated steps as described in Figure 1. For $\Phi \in \mathbb{R}^{M \times N}$ and $X \in \mathbb{R}^M$, we can analyze the time complexity as follows:

- Steps (4 and 22) convert the image block to a vector and vice versa and each one requires $\sqrt{M}$ operations, so, its complexity is $\mathcal{O}(\sqrt{M})$.
- Step (5), the inner product has complexity of $\mathcal{O}(M)$.
- Steps (7, 15), the mean and variance calculations of SSIM requires M multiplications and additions per iteration. So, for the k iterations, the complexity becomes $\mathcal{O}(kM)$.
- Step (9), here, the inner product is repeated N times, so the complexity is $\mathcal{O}(MN)$, but for the k iterations, it becomes $\mathcal{O}(kMN)$. As for the selection process, it needs N operations whose complexity is $\mathcal{O}(N)$, and for the k iterations, it becomes $\mathcal{O}(kN)$.
- Step (10) is the most complex step in OMP. For the matrix-matrix multiplication, the complexity is $\mathcal{O}(sM)$. As for the matrix-inverse, the complexity is $\mathcal{O}(s^3)$. But, for the k iterations, these complexity levels become $\mathcal{O}(k^2M)$ and $\mathcal{O}(k^4)$ respectively.

procedure nOMP(IMG,SI_{th},Φ,k, $\Delta\alpha$, e_{th})
  $B \leftarrow toBatches(IMG)$ ▷ Convert IMG to a matrix of batches
  for all $B(i,j) \in B$ **do**
    $X \leftarrow toVector(B(i,j))$
    $X_{dc} = \left(\varphi_{dc}^T X\right)\varphi_{dc}$
    $I \leftarrow \{\emptyset\}$, $r^0 \leftarrow X - X_{dc}$, $X_n \leftarrow X_{dc}$, $X_o \leftarrow X_{dc}$, $s = 0$ ▷ initialization
    while $s <= k$ AND $SI(X, X_o) <= SI_{th}$ **do**
      $s \leftarrow s + 1$
      $I \leftarrow I \cup \underset{z,\forall\varphi_z\in\Phi}{\operatorname{argmax}} \left|\varphi_z^T r_{omp}^{s-1}\right|$
      $C_o \leftarrow \left(\Phi_I^T\Phi_I\right)^{-1}\Phi_I^T X$
      $X_o \leftarrow X_{dc} + \Phi_I^T C_o$
      $r_{omp}^s \leftarrow X - X_o$
      if $SI(X, X_o) <= 0.95SI_{th}$ **then**
        $\alpha \leftarrow 1, C_n \leftarrow C_o,$
        while $SI(X, X_n) - SI(X, X_o) >= 0$ AND $\alpha <= \sqrt{e_{th}} + 1$ **do**
          $\alpha \leftarrow \alpha + \Delta\alpha$
          $C_n \leftarrow \alpha C_o$
          $X_n \leftarrow X_{dc} + \Phi_I^T C_n$
        end while
      end if
    end while
    $\hat{B}(i,j) \leftarrow toBatch(X_n)$
  end for
end procedure

FIGURE 1. nOMP methodology.

- Steps (11, 12), each step requires M operations, so, the complexity is $\mathcal{O}(M)$, and for the k iterations, the complexity becomes $\mathcal{O}(kM)$.
- Step (16), it requires a single operation which is repeated $\frac{\sqrt{e_{th}}+1}{\Delta\alpha}$ times. So, the complexity is $\mathcal{O}(\frac{\sqrt{e_{th}}+1}{\Delta\alpha})$, and for the k iterations, it becomes $\mathcal{O}(k\frac{\sqrt{e_{th}}+1}{\Delta\alpha})$.
- Step (17), it requires s multiplications which are repeated $\frac{\sqrt{e_{th}}+1}{\Delta\alpha}$ times. So, the complexity is $\mathcal{O}(s\frac{\sqrt{e_{th}}+1}{\Delta\alpha})$. But, for the k iterations, the complexity becomes $\mathcal{O}(k^2\frac{\sqrt{e_{th}}+1}{\Delta\alpha})$.
- Finally, Step (18) requires sM multiplications which are repeated $\frac{\sqrt{e_{th}}+1}{\Delta\alpha}$ times. So, the complexity is $\mathcal{O}(sM\frac{\sqrt{e_{th}}+1}{\Delta\alpha})$. But, for the k iterations, the complexity becomes $\mathcal{O}(k^2M\frac{\sqrt{e_{th}}+1}{\Delta\alpha})$.

Summing up, the overall complexity of the OMP could be concluded to be $\mathcal{O})(kMN)$ as stated in an earlier work [31]. As for the nOMP methodology, its complexity could be shortly written as $\mathcal{O}(k^2M\frac{\sqrt{e_{th}}+1}{\Delta\alpha})$.

IV. SIMULATION STUDY

Some studies tend to reconstruct noise or interference actively, and then obtain a purer original signal by removing the reconstructed interference signal from the received signal. But, in this study, the source of noise is the sparse modeling itself, hence, the proposed approach and others will try to enhance the image quality from the point of view of SSIM. To validate the effectiveness of the proposed method, three experiments are conducted.

- **In Experiment 1,** while a sparseness-based sparse representation by OMP is carried out, a comparison between iOMP and nOMP is conducted.
- **In Experiment 2,** while a SSIM-based sparse representation by OMP is carried out, a comparison between iOMP and nOMP is conducted.
- **In Experiment 3,** while a SSIM-based sparse representation by OMP is carried out, a comparison between iOMP, MiOMP, nOMP is conducted. Also, hybrid techniques are taken into account such as OMP-BM3D, OMP-TVL1, OMP-SBATV, OMP-Bilateral, nOMP-BM3D, nOMP-TVL1, nOMP-SBATV and nOMP-Bilateral., when BM3D [32], TVL1 [33], SBATV [34] and Bilateral [35] are classic enhancement techniques.

The prerequisites of this study are two sets of images, the training and testing sets. Here, the 512×512 training images shown in Figure 2 are utilized by the MOD method [36] to generate a data-dependent atoms (DDA). The DDA is a large and overcomplete set of non-orthogonal basis functions. On the other side, there is another type of atoms which is called data-independent atoms (DIA). This type of dictionaries are mathematically based such as "Discrete Cosine Transform basis (DCT)." Here, DIA is a quasi-orthogonal set of atoms which is required to study the effect of this type of atoms on the performance of the proposed algorithm. As for the testing set, as shown in Figure 3 and Figure 4, it consists of two groups of images, 256×256 images "person (IMG1), and monkey's face (IMG2) which are selected from the CVG-UGR dataset [37]. Besides this group, this study uses two satellite images, a Sentinel-1 data (SAR image) and a Sentinel-2 data (optical image) which were provided by the Egyptian National Authority for Remote Sensing and Space Sciences (NARSS).

For the numerical results, we mainly focus on the following performance metrics:

1) This study uses the Global-SSIM (GSI) to validate the performance of methodologies. The GSI could be calculated as follows:

$$GSI = \frac{1}{m}\sum_{i=1}^{m} LSI_i \tag{15}$$

where LSI_i is the Local-SSIM value of the i^{th} image block, and m is the number of 8×8 blocks. So, the GSI is considered the mean value of the local SSIM values.

2) Also, in this study, another metric known as the Normalized Mean Squared Error Ratio, or "NMSE ratio" is employed to validate the effect of a methodology **M** on the errors obtained by **OMP**. This metric can be

FIGURE 2. Training set.

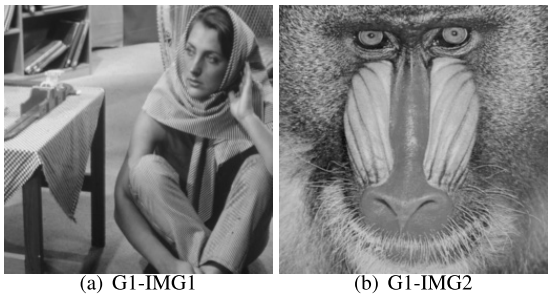

(a) G1-IMG1 (b) G1-IMG2

FIGURE 3. Testing set (group 1): 256 × 256 images.

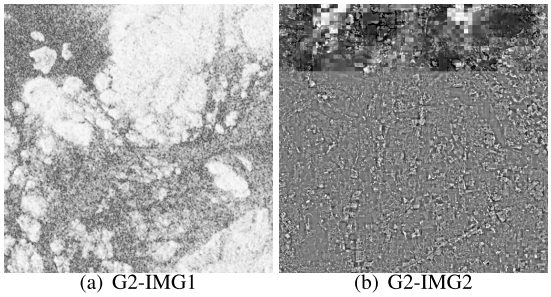

(a) G2-IMG1 (b) G2-IMG2

FIGURE 4. Testing set (group 2): 512 × 512 images.

computed as follows:

$$\text{NMSE ratio} = \frac{\text{NMSE}_{\text{OMP}}}{\text{NMSE}_{\text{M}}} \tag{16}$$

$$= \frac{\|X - X_{OMP}\|_2^2 / \|X\|_2^2}{\|X - X_M\|_2^2 / \|X\|_2^2} \tag{17}$$

$$= \frac{\|X - X_{OMP}\|_2^2}{\|X - X_M\|_2^2} \tag{18}$$

3) Like previous metric, the PSNR ratios is used and can be computed as follows:

$$\text{PSNR ratio} = \frac{\text{PSNR}_{\text{OMP}}}{\text{PSNR}_{\text{M}}} \tag{19}$$

4) In addition to the foregoing, we have conducted the student t-test at a level of 0.05 to investigate whether the out-performances are significant. All significant changes are highlighted in **bold**.

A. EXPERIMENT 1: SPARSENESS-BASED STOPPING CRITERION

1) GSI RESULTS

In this case study, all algorithms do the iterations till the sparseness level reaches a predefined level. So, all image blocks will be modeled sparsely at the same level. Table 1 shows the GSI values of OMP, iOMP and nOMP for the group 1 of images. As shown, for G1-IMG1, the GSI values of DIA increase gradually per iteration by about 7.23%, 6.25% and 7.28% for OMP, iOMP and nOMP respectively. Comparing to the conventional OMP, iOMP gives values for the GSI which are less than that of OMP by approximately 5.18%, but nOMP enhanced these values slightly by approximately 0.55%.

As for the results of DDA, the GSI values increase gradually per iteration by about 8.18%, 8.13% and 8.24% for OMP, iOMP and nOMP respectively. Comparing to the conventional OMP, iOMP gives values for the GSI which are less than that of OMP by approximately 0.59%, but nOMP enhanced these values slightly by approximately 0.3%.

For G1-IMG2, the GSI values of DIA increase gradually per iteration by about 8.9%, 7.15% and 8.99% for OMP, iOMP and nOMP respectively. Comparing to the conventional OMP, iOMP gives values for the GSI which are less than that of OMP by approximately 9.06%, but nOMP enhanced these values by approximately 0.98%. As for the results of DDA, the GSI values increase gradually per iteration by about 9.7%, 9.59% and 9.83% for OMP, iOMP and nOMP respectively. Comparing to the conventional OMP, iOMP gives values for the GSI which are less than that of OMP by approximately 1.29%, but nOMP enhanced these values by approximately 0.77%.

For G2-IMG1, the GSI values of DIA increase gradually per iteration by about 10.79%, 8.67% and 10.95% for OMP, iOMP and nOMP respectively. Comparing to the conventional OMP, iOMP gives values for the GSI which are less than that of OMP by approximately 11.73%, but nOMP enhanced these values significantly by about 1.47%. As for the results of DDA, the GSI values increase gradually

TABLE 1. Results of group 1.

	Data Independent Atoms (DIA)								Data Dependent Atoms (DDA)							
	G1-IMG1 (Woman)				G1-IMG2 (Monkey)				G1-IMG1 (Woman)				G1-IMG2 (Monkey)			
k	OMP	iOMP	nOMP	t-test (p)	OMP	iOMP	nOMP	t-test (p)	OMP	iOMP	nOMP	t-test (p)	OMP	iOMP	nOMP	t-test (p)
1	0.478	0.478	0.478	*>0.05*	0.388	0.388	0.388	*>0.05*	0.478	0.478	0.478	*>0.05*	0.388	0.388	0.388	*>0.05*
2	0.638	0.642	0.649	*>0.05*	0.535	0.538	0.545	*>0.05*	0.774	0.776	0.781	*>0.05*	0.614	0.620	0.627	*>0.05*
3	0.725	0.716	0.734	*>0.05*	0.621	0.601	0.632	*>0.05*	0.834	0.828	0.838	*>0.05*	0.699	0.693	0.709	*>0.05*
4	0.780	0.753	0.785	*>0.05*	0.678	0.636	0.688	*>0.05*	0.866	0.860	0.869	*>0.05*	0.751	0.738	0.758	*>0.05*
5	0.818	0.775	0.822	*>0.05*	0.723	0.661	0.731	*>0.05*	0.887	0.881	0.889	*>0.05*	0.789	0.773	0.794	*>0.05*
6	0.847	0.794	0.850	*>0.05*	0.761	0.680	0.767	*>0.05*	0.902	0.895	0.904	*>0.05*	0.816	0.801	0.820	*>0.05*
7	0.870	0.810	0.872	*>0.05*	0.791	0.699	0.796	*>0.05*	0.914	0.907	0.915	*>0.05*	0.838	0.824	0.842	*>0.05*
8	0.889	0.823	0.890	*>0.05*	0.817	0.707	0.821	*>0.05*	0.923	0.917	0.925	*>0.05*	0.856	0.842	0.859	*>0.05*
9	0.905	0.832	0.906	*>0.05*	0.839	0.721	0.842	*>0.05*	0.931	0.925	0.932	*>0.05*	0.870	0.857	0.872	*>0.05*
10	0.918	0.838	0.919	*>0.05*	0.857	0.734	0.860	*>0.05*	0.936	0.931	0.937	*>0.05*	0.883	0.870	0.885	*>0.05*

TABLE 2. Results of group 2.

	Data Independent Atoms (DIA)								Data Dependent Atoms (DDA)							
	G2-IMG1 (Sentinel-1 SAR image)				G2-IMG2 (Sentinel-2 Opt image)				G2-IMG1 (Sentinel-1 SAR image)				G2-IMG2 (Sentinel-2 Opt image)			
k	OMP	iOMP	nOMP	t-test (p)	OMP	iOMP	nOMP	t-test (p)	OMP	iOMP	nOMP	t-test (p)	OMP	iOMP	nOMP	t-test (p)
1	0.332	0.332	0.332	*>0.05*	0.255	0.255	0.255	*>0.05*	0.332	0.332	0.332	*>0.05*	0.255	0.255	0.255	*>0.05*
2	0.490	0.497	**0.505**	*<0.05*	0.420	0.430	**0.435**	*<0.05*	0.595	0.609	**0.613**	*<0.05*	0.543	0.555	**0.561**	*<0.05*
3	0.588	0.561	**0.605**	*<0.05*	0.531	0.515	**0.548**	*<0.05*	0.696	0.692	**0.708**	*<0.05*	0.652	0.646	**0.664**	*<0.05*
4	0.656	0.596	**0.670**	*<0.05*	0.610	0.575	**0.624**	*<0.05*	0.756	0.745	**0.765**	*<0.05*	0.722	0.708	**0.730**	*<0.05*
5	0.707	0.622	**0.719**	*<0.05*	0.668	0.617	**0.679**	*<0.05*	0.797	0.784	**0.804**	*<0.05*	0.773	0.756	**0.779**	*<0.05*
6	0.747	0.642	**0.756**	*<0.05*	0.716	0.652	**0.722**	*<0.05*	0.828	0.814	**0.833**	*<0.05*	0.811	0.794	**0.815**	*<0.05*
7	0.780	0.660	**0.787**	*<0.05*	0.755	0.678	**0.761**	*<0.05*	0.851	0.838	**0.855**	*<0.05*	0.842	0.824	0.844	*>0.05*
8	0.807	0.675	**0.813**	*<0.05*	0.788	0.703	**0.793**	*<0.05*	0.870	0.857	**0.873**	*<0.05*	0.866	0.849	0.868	*>0.05*
9	0.831	0.688	**0.835**	*<0.05*	0.816	0.724	**0.819**	*<0.05*	0.884	0.872	0.887	*>0.05*	0.885	0.870	0.887	*>0.05*
10	0.851	0.697	0.854	*<0.05*	0.840	0.743	0.843	*>0.05*	0.896	0.885	0.898	*>0.05*	0.901	0.887	0.902	*>0.05*

per iteration by about 12.34%, 12.35% and 12.57% for OMP, iOMP and nOMP respectively. Comparing to the conventional OMP, iOMP gives values for the GSI which are less than that of OMP by approximately 0.98%, but nOMP enhanced these values by approximately 0.97%.

For G2-IMG2, the GSI values of DIA increase gradually per iteration by about 14.15%, 12.84% and 14.38% for OMP, iOMP and nOMP respectively. Comparing to the conventional OMP, iOMP gives values for the GSI which are less than that of OMP by approximately 7.4%, but nOMP enhanced these values by approximately 1.56%. As for the results of DDA, the GSI values increase gradually per iteration by about 16.81%, 16.85% and 17.15% for OMP, iOMP and nOMP respectively. Comparing to the conventional OMP, iOMP gives values for the GSI which are less than that of OMP by approximately 1.38%, but nOMP enhanced these values by approximately 0.92%.

On average, it could be seen that, the GSI values of DIA increase gradually per iteration by about 10.27%, 8.73% and 10.4% for OMP, iOMP and nOMP respectively. Comparing to the conventional OMP, iOMP gives values for the GSI which are less than that of OMP by approximately 8.34%, but nOMP enhanced these values significantly by about 1.14%. As for the results of DDA, the GSI values increase gradually per iteration by about 11.76%, 11.73% and 11.95% for OMP, iOMP and nOMP respectively. Comparing to the conventional OMP, iOMP gives values for the GSI which are less than that of OMP by approximately 1.06%, but nOMP enhanced these values by approximately 0.74%. Also, it could be observed that, iOMP is always better than OMP after selecting the first ac coefficient, then, its performance degrades gradually.

2) NMSE RATIOS AND VISUAL RESULTS

As for the NMSE ratios for iOMP and nOMP, these are shown in Figure 5. As can be seen, although the quality enhancement acquired by nOMP, both iOMP and nOMP result in more errors in terms of the NMSE. But, nOMP gives NMSE levels close to that of OMP. For (Group 1, DDA), see Figure 5(a), the NMSE ratios are 0.906 and 0.964 for iOMP and nOMP respectively. But for (Group 1, DIA), see Figure 5(b), these ratios become 0.718 and 0.958 for iOMP and nOMP respectively.

With regard to (Group 2, DDA), see Figure 5(c), the NMSE ratios are 0.873 and 0.951 for iOMP and nOMP respectively. But for (Group 2, DIA), see Figure 5(d), these ratios become 0.712 and 0.936 for iOMP and nOMP respectively.

On average, in terms of the NMSE ratios, nOMP is closer to OMP than iOMP. As can be seen, the NMSE ratios of nOMP are approximately 0.95, and the NMSE ratios of iOMP are approximately 0.8.

Some visual results for the "Sentinel-2 Opt image" are shown in Figure 6.

B. EXPERIMENT 2: SSIM-BASED STOPPING CRITERION

Now, another case study is considered, when the stopping criterion becomes the local SSIM level rather than the sparseness level. This experiment illustrates how much image

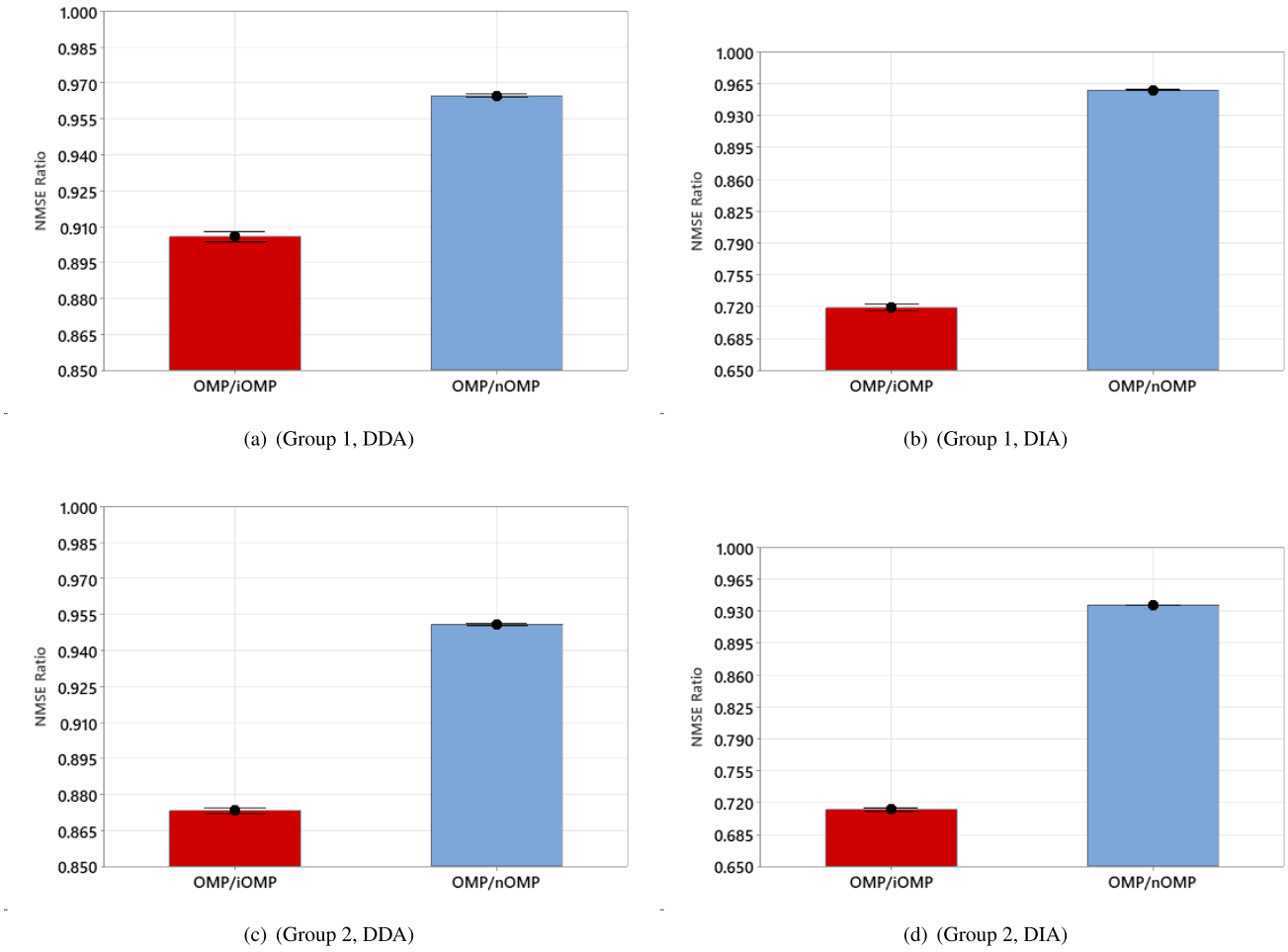

FIGURE 5. Average result of NMSE ratios for the images in group 1 and group 2.

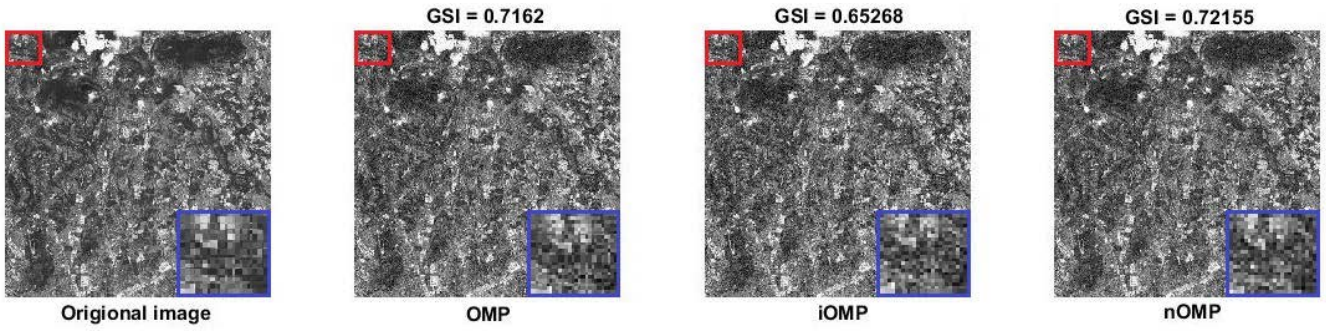

FIGURE 6. Visual results of the Sentinel-2 Opt image, 512 × 512 , $k = 6$, DIA.

batches get more sparse at the same GSI level. In other words, how much GSI level gets more better at the same sparseness level. The results shown in Figure 7 measures how much the GSI level is increased when the obtained average sparseness level is $k = 4$. Compared to the GSI levels obtained by the sparseness-based methods (at k = 4) using the data-independent atoms, OMP shows GSI enhancements by approximately 3.22%, 2.31%, 3.23% and 2.61% for G1-IMG1, G1-IMG2, G2-IMG1 and G2-IMG2 respectively. But iOMP shows enhancements by 0.25%, 0.54%, 1.28% and 1.72% for G1-IMG1, G1-IMG2, G2-IMG1 and G2-IMG2 respectively. As for nOMP, the enhancements become 2.96%, 2.14%, 2.87% and 2.62% for G1-IMG1, G1-IMG2, G2-IMG1 and G2-IMG2 respectively.

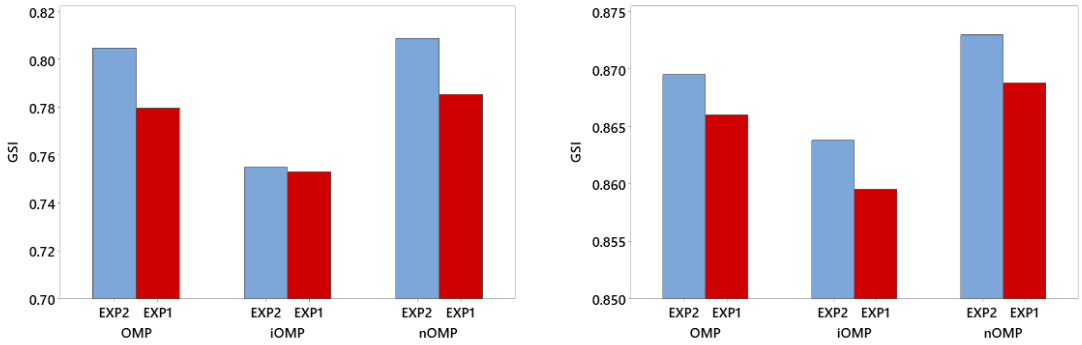

(a) G1-IMG1, DIA

(b) G1-IMG1, DDA

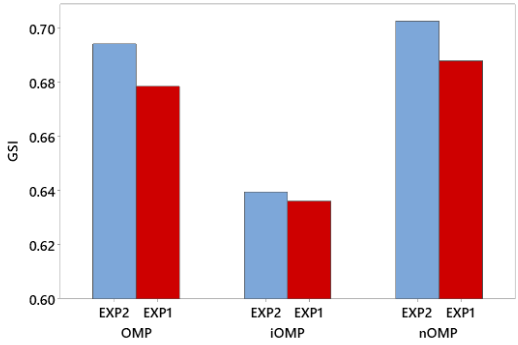

(c) G1-IMG2, DIA

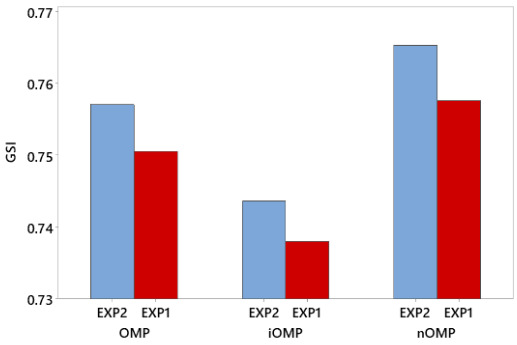

(d) G1-IMG2, DDA

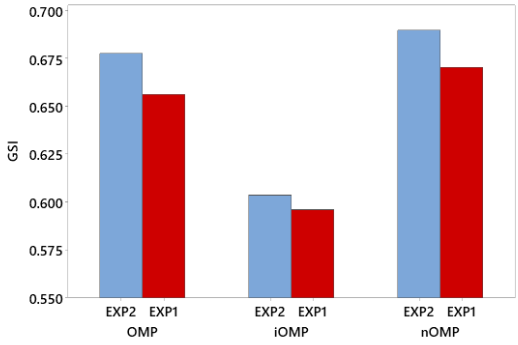

(e) G2-IMG1, DIA

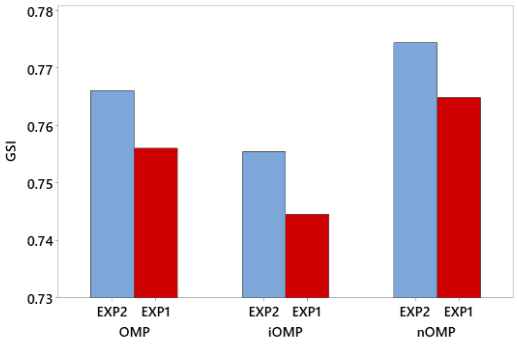

(f) G2-IMG1, DDA

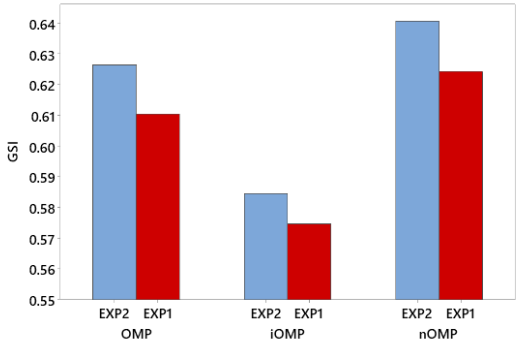

(g) G2-IMG2, DIA

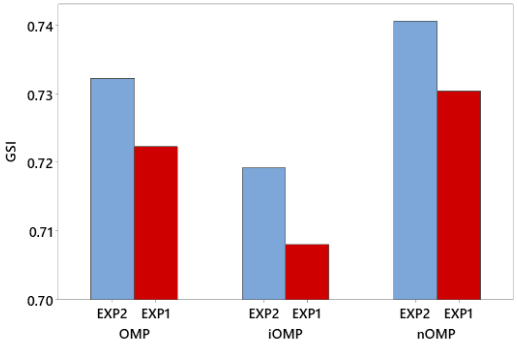

(h) G2-IMG2, DDA

FIGURE 7. Results of second experiment, GSI level at $k_{avg} = 4$.

TABLE 3. Average results of the SIPI dataset, size 128 × 128.

		One stage				Two stages							
	k	OMP	iOMP	MiOMP	nOMP	OMP-BM3D	OMP-TVL1	OMP-SBATV	OMP-Bilateral	nOMP-BM3D	nOMP-TVL1	nOMP-SBATV	nOMP-Bilateral
DDA	2	0.53	0.54	0.55	0.55	0.51	0.50	0.51	0.40	**0.54**	0.53	**0.54**	0.47
	4	0.72	0.71	**0.73**	**0.73**	**0.74**	**0.73**	**0.74**	0.67	**0.75**	**0.75**	**0.75**	0.72
	6	0.81	0.79	**0.82**	0.81	**0.84**	**0.83**	**0.84**	0.80	**0.84**	**0.84**	**0.84**	**0.83**
	8	0.86	0.84	**0.87**	0.86	**0.89**	**0.88**	**0.89**	**0.87**	**0.89**	**0.88**	**0.89**	**0.88**
	10	0.89	0.88	0.90	**0.90**	**0.92**	**0.91**	**0.92**	**0.91**	**0.92**	**0.91**	**0.92**	**0.91**
	12	0.92	0.91	0.92	0.92	**0.94**	**0.93**	**0.94**	**0.93**	**0.94**	**0.93**	**0.94**	**0.94**
DIA	2	0.46	0.47	**0.48**	**0.48**	0.46	0.45	0.46	0.35	**0.49**	**0.48**	**0.49**	0.43
	4	0.64	0.58	**0.65**	**0.65**	**0.65**	**0.66**	**0.67**	0.55	**0.67**	**0.68**	**0.69**	0.63
	6	0.74	0.64	0.74	**0.75**	**0.76**	**0.76**	**0.77**	0.70	**0.77**	**0.78**	**0.78**	**0.75**
	8	0.80	0.68	**0.81**	**0.81**	**0.82**	**0.82**	**0.84**	0.79	**0.83**	**0.83**	**0.84**	**0.82**
	10	0.85	0.71	0.85	0.85	**0.88**	**0.86**	**0.88**	**0.86**	**0.88**	**0.87**	**0.88**	**0.87**
	12	0.89	0.73	0.89	0.89	**0.91**	0.89	**0.91**	**0.90**	**0.91**	**0.90**	**0.91**	**0.91**

On the other side, for the data-dependent atoms at the same sparseness level, these results changed dramatically as follows: OMP gives enhancements by approximately 0.4%, 0.86%, 1.33% and 1.37% for G1-IMG1, G1-IMG2, G2-IMG1 and G2-IMG2 respectively. But iOMP shows enhancements by 0.5%, 0.76%, 1.46% and 1.6% for G1-IMG1, G1-IMG2, G2-IMG1 and G2-IMG2 respectively. Finally, nOMP gives enhancements by approximately 0.48%, 1.02%, 1.25% and 1.4% for G1-IMG1, G1-IMG2, G2-IMG1 and G2-IMG2 respectively.

On average, it could be seen that, the obtained enhancements are 1.92%, 1.01% and 1.84% for OMP, iOMP and nOMP respectively, and nOMP still outperforms both OMP and iOMP.

C. EXPERIMENT 3: COMPARISON TO MIOMP AND HYBRID TECHNIQUES

In this section, to validate the performance of nOMP, another experiment is conducted on a huge number of images belonging to the USC-SIPI dataset (40 images) [38] and a Sentinel-1 dataset (40 images). In this experiment, iOMP and nOMP are compared to MiOMP [30]. Besides that, a comparison is conducted with another hybrid techniques, in which, a post enhancement stage is added to OMP and nOMP to make extra-enhancements. These are entitled OMP-BM3D, OMP-TVL1, OMP-SBATV, OMP-Bilateral, nOMP-BM3D, nOMP-TVL1, nOMP-SBATV and nOMP-Bilateral. Moreover, in this experiment, the image size is another factor which is utilized to validate the performance of all algorithms. For both datasets we have used two sizes 128×128 and 64×64. Note that, all bold values shown in the tables represent significant change in the OMP GSI values according to the t-test.

1) AVERAGE RESULTS OF USC-SIPI DATASET (128×128)

Table 3 shows the average results of the USC-SIPI dataset. As observed before in [30], iOMP doesn't exhibit whether significant or non-significant enhancements, in other words, all GSI levels of iOMP are below that of OMP. But, it is also noted that, iOMP gives a unique enhancement at $k = 2$. In other words, iOMP works better than OMP if and only if there is no more than one ac coefficient.

a: EFFECT OF NON-HYBRID TECHNIQUES ON THE GSI LEVELS OF OMP

As can be seen, while iOMP doesn't make any improvements, MiOMP and nOMP do. The acquired improvements by MiOMP and nOMP are 1.82% and 1.57% respectively, when the DDA-based dictionary is used. But, for the DIA-based dictionary, these improvements become 1.21% and 1.49% respectively.

b: EFFECT OF CLASSIC ENHANCEMENTS ON THE PERFORMANCE

With the exception of Bilateral method, which performs well at greater sparseness levels, conventional methods demonstrate large changes in GSI levels of both OMP and nOMP at most sparseness levels.

The obtained enhancements for DDA and DIA dictionaries in OMP-BM3D are 1.85% and 2.15%, respectively. These enhancements become 0.39% and 1.51% for OMP-TVL1. The gained enhancements by OMP-SBATV are 1.74% and 3.46% respectively. On the other hand, when these traditional techniques are employed as a post-stage for nOMP, the results are improved. For nOMP-BM3D, the changes are 3.32% and 4.24% for DDA and DIA dictionaries respectively. But for nOMP-TVL1, the changes become 2.33% and 4.23%. These significant enhancements for nOMP-SBATV reach 3.23% and 5.45% respectively.

To summarize, regardless of the dictionary type, and in terms of the gains in OMP's GSI levels, it can be shown that after merging BM3D with nOMP, its performance outperforms both OMP-BM3D and nOMP by about 1.78% and 2.44%, respectively. In the case of merging TVL1 with nOMP, nOMP-TVL1 outperforms both OMP-TVL1 and nOMP by about 2.34% and 1.95%, respectively. Also, in the

TABLE 4. Average results of the SIPI dataset, size 64 × 64.

		One stage				Two stages							
	k	OMP	iOMP	MiOMP	nOMP	OMP-BM3D	OMP-TVL1	OMP-SBATV	OMP-Bilateral	nOMP-BM3D	nOMP-TVL1	nOMP-SBATV	nOMP-Bilateral
DDA	2	0.47	0.49	**0.50**	**0.49**	0.45	0.44	0.45	0.34	**0.48**	0.47	**0.48**	0.40
	4	0.65	0.64	**0.66**	**0.67**	**0.67**	0.64	**0.66**	0.56	**0.69**	**0.67**	**0.69**	0.63
	6	0.75	0.73	**0.76**	**0.76**	**0.77**	0.74	**0.77**	0.70	**0.78**	**0.76**	**0.78**	0.75
	8	0.81	0.79	0.81	0.81	**0.83**	0.80	**0.83**	0.78	**0.84**	**0.82**	**0.84**	**0.82**
	10	0.84	0.83	**0.85**	**0.85**	**0.87**	0.84	**0.87**	0.84	**0.88**	**0.85**	**0.88**	**0.86**
	12	0.87	0.86	**0.88**	**0.88**	**0.90**	0.86	**0.90**	**0.88**	**0.90**	0.87	**0.90**	**0.89**
DIA	2	0.46	**0.47**	**0.47**	**0.47**	0.45	0.42	0.45	0.33	**0.48**	0.45	**0.48**	0.41
	4	0.62	0.57	**0.63**	**0.63**	**0.64**	0.60	**0.64**	0.53	**0.67**	**0.63**	**0.67**	0.62
	6	0.71	0.62	**0.72**	**0.72**	**0.74**	0.69	**0.74**	0.66	**0.76**	**0.72**	**0.76**	**0.73**
	8	0.78	0.66	0.78	**0.79**	**0.81**	0.76	**0.81**	0.76	**0.82**	0.78	**0.82**	**0.80**
	10	0.83	0.69	0.83	0.83	**0.86**	0.80	**0.86**	0.82	**0.86**	0.82	**0.86**	**0.85**
	12	0.87	0.71	0.87	0.87	**0.89**	0.84	**0.89**	0.87	**0.89**	0.85	**0.90**	**0.88**

case of nOMP-SBATV, it outperforms both OMP-SBATV and nOMP by approximately 1.72% and 2.99%, respectively. Finally, when $k > 2$, nOMP-Bilateral outperforms OMP-Bilateral by about 3.95%, and nOMP by 0.86%.

2) AVERAGE RESULTS OF USC-SIPI DATASET (64 × 64)

Table 4 shows the average results of the USC-SIPI dataset sized 64 × 64 . As stated before, iOMP gives a unique enhancement at $k = 2$. In other words, iOMP works better than OMP if and only if there is no more than one ac coefficient.

a: EFFECT OF NON-HYBRID TECHNIQUES ON THE GSI LEVELS OF OMP:

There are no improvements obtained by iOMP, as there were in the case of 128 × 128 . But, MiOMP and nOMP achieve significant improvements. When the DDA-based dictionary is employed, MiOMP and nOMP achieve improvements of 2.18% and 2.05%, respectively. For the DIA-based dictionary, these values decrease slightly and reach 1.24% for MiOMP and 1.65% for nOMP.

b: EFFECT OF CLASSIC ENHANCEMENTS ON THE PERFORMANCE:

Unlike the case of 128 × 128 , here, the TVL1 is not effective at all, so it will be excluded from the discussion. But, Bilateral method is still working well at the high sparseness levels. On the other side, both BM3D and SBATV are working well at most levels of k.

Compared to the GSI's levels of OMP, the obtained enhancements for DDA and DIA dictionaries in OMP-BM3D are 1.69% and 2.92%, respectively. For OMP-SBATV, these values decrease to 1.46% and 2.82% respectively. On the other hand, when these conventional methods are employed as a post-stage for nOMP, the results are improved significantly. For nOMP-BM3D, the changes are 4.03% and 5.34% for DDA and DIA dictionaries, respectively. But, for nOMP-SBATV, these enhancements are 3.93% and 5.38% respectively.

To summarize, regardless of the dictionary type, and in terms of the gains in OMP's GSI levels, it can be shown that after merging BM3D with nOMP, its performance outperforms both OMP-BM3D and nOMP by about 2.37% and 2.97%, respectively. In the case of nOMP-SBATV, it outperforms both OMP-SBATV and nOMP by approximately 2.52% and 2.94%, respectively. Finally, when $k > 4$, nOMP-Bilateral outperforms OMP-Bilateral by about 5.35%, and nOMP by 0.98%.

3) AVERAGE RESULTS OF SENTINEL-1 DATA (128 × 128)

Table 5 shows the average results of the Sentinel-1 dataset. Like the observations found in USC-SIPI dataset, iOMP still works better than OMP if and only if there is no more than one ac coefficient.

a: EFFECT OF NON-HYBRID TECHNIQUES ON THE GSI LEVELS OF OMP:

As can be observed, while iOMP doesn't make any improvements, MiOMP and nOMP do. The gained improvements by MiOMP and nOMP are 1.36% and 1.15% respectively, when the DDA-based dictionary is used. But, for the DIA-based dictionary, these improvements become 0.95% and 1.22% respectively.

b: EFFECT OF CLASSIC ENHANCEMENTS ON THE PERFORMANCE:

With the exception of Bilateral method, which performs well at greater sparseness levels, conventional methods demonstrate large changes in GSI levels of both OMP and nOMP at most sparseness levels.

The obtained enhancements for DDA and DIA dictionaries in OMP-BM3D are 2.04% and 3.31%, respectively. These enhancements become 0.92% and 1.52% for OMP-TVL1. The gained enhancements by OMP-SBATV are 1.91% and 3.28% respectively. On the other hand, when these traditional

TABLE 5. Average results of the sentinel-1 dataset, size 128 × 128.

		One stage				Two stages							
	k	OMP	iOMP	MiOMP	nOMP	OMP-BM3D	OMP-TVL1	OMP-SBATV	OMP-Bilateral	nOMP-BM3D	nOMP-TVL1	nOMP-SBATV	nOMP-Bilateral
DDA	2	0.59	**0.60**	**0.60**	**0.60**	0.57	0.57	0.57	0.51	0.59	0.59	0.59	0.56
	4	0.74	0.73	**0.75**	**0.75**	**0.76**	**0.75**	**0.76**	0.71	**0.77**	**0.77**	**0.77**	**0.75**
	6	0.81	0.80	**0.82**	**0.82**	**0.84**	**0.83**	**0.84**	0.81	**0.84**	**0.84**	**0.84**	**0.83**
	8	0.85	0.84	**0.86**	**0.86**	**0.88**	**0.87**	**0.88**	**0.86**	**0.88**	**0.88**	**0.88**	**0.88**
	10	0.88	0.87	**0.89**	0.88	**0.91**	**0.90**	**0.91**	**0.90**	**0.91**	**0.90**	**0.91**	**0.91**
	12	0.90	0.89	**0.91**	0.90	**0.93**	**0.91**	**0.93**	**0.92**	**0.93**	**0.92**	**0.93**	**0.92**
DIA	2	0.49	0.49	**0.50**	**0.50**	**0.50**	**0.50**	**0.50**	0.43	**0.52**	**0.52**	**0.52**	0.49
	4	0.65	0.60	**0.66**	**0.67**	**0.68**	**0.67**	**0.68**	0.62	**0.69**	**0.69**	**0.68**	**0.67**
	6	0.74	0.65	**0.75**	**0.75**	**0.77**	**0.76**	**0.77**	0.73	**0.78**	**0.77**	**0.77**	**0.77**
	8	0.80	0.68	**0.81**	**0.81**	**0.83**	**0.81**	**0.83**	0.80	**0.83**	**0.82**	**0.83**	**0.83**
	10	0.85	0.70	0.85	0.85	**0.87**	0.85	**0.87**	0.85	**0.87**	**0.86**	**0.87**	**0.87**
	12	0.88	0.72	0.88	0.88	**0.90**	0.88	**0.90**	**0.89**	**0.90**	**0.89**	**0.90**	**0.90**

TABLE 6. Average results of the sentinel-1 SAR dataset, size 64 × 64.

		One stage				Two stages							
	k	OMP	iOMP	MiOMP	nOMP	OMP-BM3D	OMP-TVL1	OMP-SBATV	OMP-Bilateral	nOMP-BM3D	nOMP-TVL1	nOMP-SBATV	nOMP-Bilateral
DDA	2	0.56	**0.57**	**0.57**	**0.57**	0.55	0.55	0.55	0.49	**0.57**	**0.57**	**0.57**	0.54
	4	0.72	0.71	**0.73**	**0.73**	**0.74**	**0.73**	**0.74**	0.69	**0.75**	**0.75**	**0.75**	**0.73**
	6	0.80	0.79	**0.81**	**0.80**	**0.83**	**0.81**	**0.82**	0.80	**0.83**	**0.82**	**0.83**	**0.82**
	8	0.85	0.84	**0.86**	0.85	**0.87**	**0.86**	**0.87**	**0.86**	**0.88**	**0.87**	**0.87**	**0.87**
	10	0.88	0.87	**0.89**	0.88	**0.90**	**0.89**	**0.90**	**0.89**	**0.91**	**0.89**	**0.90**	**0.90**
	12	0.90	0.89	**0.91**	**0.91**	**0.92**	**0.91**	**0.92**	**0.92**	**0.92**	**0.91**	**0.92**	**0.92**
DIA	2	0.47	0.48	**0.49**	**0.49**	**0.48**	**0.48**	**0.48**	0.41	**0.50**	**0.50**	**0.50**	0.46
	4	0.63	0.57	**0.64**	**0.65**	**0.67**	**0.65**	**0.67**	0.60	**0.68**	**0.67**	**0.68**	**0.66**
	6	0.73	0.62	**0.73**	**0.74**	**0.76**	**0.75**	**0.76**	0.71	**0.77**	**0.76**	**0.77**	**0.75**
	8	0.79	0.66	**0.80**	**0.80**	**0.82**	**0.80**	**0.82**	0.79	**0.82**	**0.81**	**0.83**	**0.81**
	10	0.84	0.68	0.84	0.84	**0.86**	0.84	**0.86**	0.84	**0.87**	**0.85**	**0.87**	**0.86**
	12	0.87	0.70	0.87	0.88	**0.89**	0.87	**0.89**	**0.88**	**0.89**	**0.88**	**0.90**	**0.89**

techniques are employed as a post-stage for nOMP, the results are improved. For nOMP-BM3D, the changes are 3.09% and 4.64% for DDA and DIA dictionaries respectively. But for nOMP-TVL1, the changes become 2.28% and 3.41%. These significant enhancements for nOMP-SBATV reach 2.71% and 4.24% respectively. As for nOMP-Bilateral, these values become 1.02% and 2.32% respectively.

To summarize, regardless of the dictionary type, and in terms of the gains in OMP's GSI levels, it can be shown that after merging BM3D with nOMP, its performance outperforms both OMP-BM3D and nOMP by about 1.17% and 2.79%, respectively. In the case of merging TVL1 with nOMP, nOMP-TVL1 outperforms both OMP-TVL1 and nOMP by about 1.61% and 1.78%, respectively. Also, in the case of nOMP-SBATV, it outperforms both OMP-SBATV and nOMP by approximately 0.87% and 2.41%, respectively. Finally, when $k > 2$, nOMP-Bilateral outperforms OMP-Bilateral by about 2.87%, and nOMP by 1.77%.

4) AVERAGE RESULTS OF SENTINEL-1 DATA (64 × 64)

Table 6 shows the average results of the Sentinel-1 dataset. Like the observations found in USC-SIPI dataset, iOMP still works better than OMP if and only if there is no more than one ac coefficient.

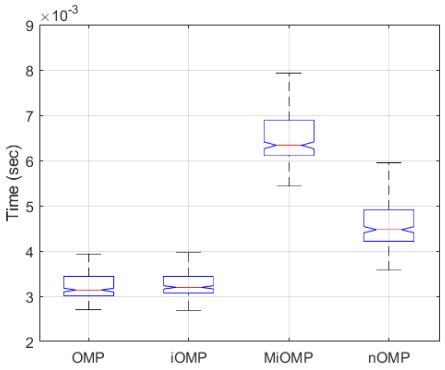

FIGURE 8. Average computation time per sparseness level.

a: EFFECT OF NON-HYBRID TECHNIQUES ON THE GSI LEVELS OF OMP:

As can be observed, while iOMP doesn't make any improvements, MiOMP and nOMP do. The gained improvements by MiOMP and nOMP are 1.31% and 1.07% respectively, when

TABLE 7. Average results of NMSE ratios for Experiment 3.

		iOMP	MiOMP	nOMP	OMP-BM3D	OMP-TVL1	OMP-SBATV	OMP-Bilateral	nOMP-BM3D	nOMP-TVL1	nOMP-SBATV	nOMP-Bilateral
USC-SIPI	128 x 128	0.532	0.944	0.920	0.974	0.950	1.004	0.887	0.900	0.920	0.885	0.942
	64 x 64	0.562	0.936	0.914	1.001	0.885	1.006	0.887	0.916	0.871	0.903	0.963
Sentinel-1	128 x 128	0.586	0.952	0.912	1.013	0.941	0.812	0.969	0.928	0.887	0.549	1.009
	64 x 64	0.598	0.961	0.923	1.006	0.939	0.809	0.953	0.934	0.888	0.535	0.989

TABLE 8. Average results of PSNR ratios for experiment 3.

		iOMP	MiOMP	nOMP	OMP-BM3D	OMP-TVL1	OMP-SBATV	OMP-Bilateral	nOMP-BM3D	nOMP-TVL1	nOMP-SBATV	nOMP-Bilateral
USC-SIPI	128 x 128	1.030	1.000	1.100	1.000	1.014	1.000	1.015	1.097	1.080	1.099	1.057
	64 x 64	1.020	1.004	1.009	1.000	1.015	1.000	1.014	1.008	1.017	1.007	1.006
Sentinel-1	128 x 128	1.022	1.000	1.131	0.999	1.009	0.999	1.009	1.122	1.128	1.156	1.088
	64 x 64	1.020	1.003	1.008	1.000	1.012	1.000	1.009	1.007	1.016	1.009	1.004

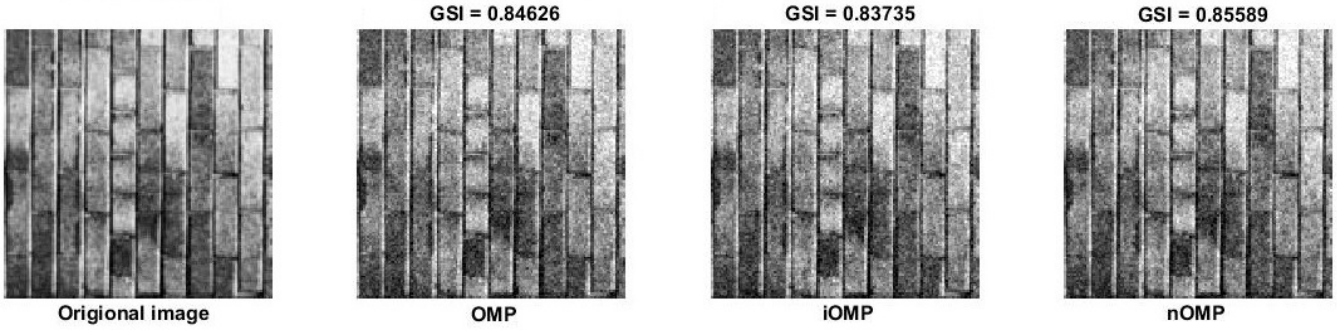

FIGURE 9. Visual results of an image belonging to USC-SIPI dataset, 128 × 128 , $k = 6$, DDA.

the DDA-based dictionary is used. But, for the DIA-based dictionary, these improvements become 0.83% and 1.14% respectively.

b: EFFECT OF CLASSIC ENHANCEMENTS ON THE PERFORMANCE:

With the exception of Bilateral method, which performs well at greater sparseness levels, conventional methods demonstrate large changes in GSI levels of both OMP and nOMP at most sparseness levels.

The obtained enhancements for DDA and DIA dictionaries in OMP-BM3D are 2.07% and 3.28%, respectively. These enhancements become 0.71% and 1.33% for OMP-TVL1. The gained enhancements by OMP-SBATV are 1.86% and 3.39% respectively. On the other hand, when these traditional techniques are employed as a post-stage for nOMP, the results are improved. For nOMP-BM3D, the changes are 3.13% and 4.74% for DDA and DIA dictionaries respectively. But for nOMP-TVL1, the changes become 2.1% and 3.37%. These significant enhancements for nOMP-SBATV reach 2.72% and 4.65% respectively. As for nOMP-Bilateral, these values become 0.81% and 1.72% respectively.

To summarize, regardless of the dictionary type, and in terms of the gains in OMP's GSI levels, it can be shown that after merging BM3D with nOMP, its performance outperforms both OMP-BM3D and nOMP by about 1.23% and 2.94%, respectively. In the case of merging TVL1 with nOMP, nOMP-TVL1 outperforms both OMP-TVL1 and nOMP by about 1.7% and 1.75%, respectively. Also, in the case of nOMP-SBATV, it outperforms both OMP-SBATV and nOMP by approximately 1.04% and 2.69%, respectively. Finally, when $k > 2$, nOMP-Bilateral outperforms OMP-Bilateral by about 2.94%, and nOMP by 1.51%.

5) AVERAGE RESULTS OF (NMSE, PSNR) RATIOS AND VISUAL RESULTS

Table 7 shows the average results of the NMSE ratios for all algorithms. As can be observed, nOMP is still outperform iOMP because nOMP's errors are closer to OMP's errors than that of iOMP. But, MiOMP is more closer to OMP than both nOMP and iOMP. As for the hybrid techniques, both BM3D and Bilateral versions of nOMP are closer to OMP than nOMP, but the Bilateral version only ouperforms MiOMP. As for the PSNR ratios, these are shown in Table 8.

Finally, some visual results for two images belonging to the USC-SIPI and Sentinel-1 datasets are shown in Figure 10 and Figure 9 respectively.

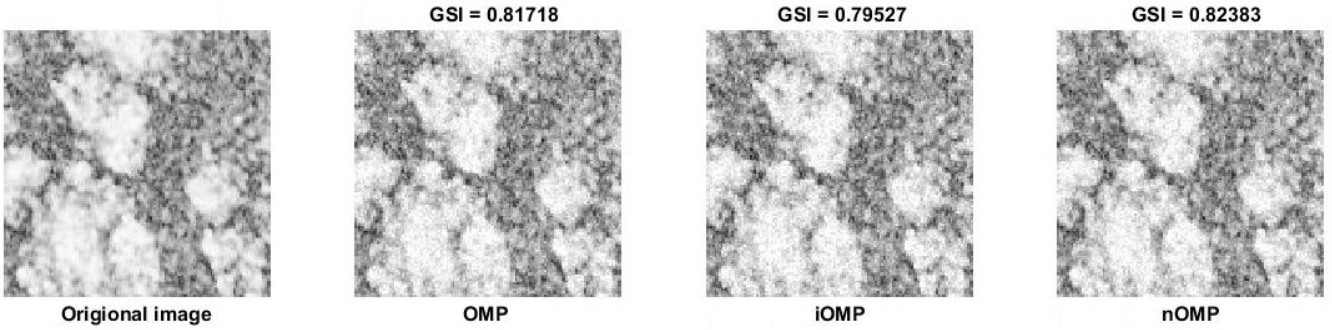

FIGURE 10. Visual results of an image belonging to Sentinel-1 dataset, 128 × 128 , $k = 6$, DDA.

6) COMPUTATION TIME

In terms of execution time, the proposed method's code is written in Matlab R2018b. The tests are run on a machine with an Intel Core i7 processor and 8 GB of RAM. The average computation time of OMP, iOMP, MiOMP, and nOMP is shown in Figure 8. The running times depicted are the amount of time spent on a single iteration. It can be shown that nOMP performs better than MiOMP. In nOMP, one iteration takes 4.4 milliseconds, but in MiOMP, one iteration takes 6.3 milliseconds. It can also be shown that the time used by MiOMP's iteration equals the sum of the times taken by both OMP and iOMP algorithms.

V. CONCLUSION

This paper's main contribution is an iterative solution for promoting the structural similarity index levels of sparseness-based encoded images. Unlike MSE-based enhancement techniques, this methodology is built on SSIM and delivers the highest SSIM regardless of the MSE levels obtained. The proposed method is a novel iterative method that acts as a modifier for OMP's sparse coefficient.

Like the work [29], our approach presumes implicitly that the old coefficients are directly proportional to the new ones. But, unlike it, nOMP considers each forward sparse iteration as a standalone stage ''isolation'' that doesn't affect on the next iterations. This type of isolation enables us to ensure the enhancement process by comparing our results with the non-modified OMP. Also, our approach is iterative-based that modifies the coefficients iteratively, and this task avoids the single-differentiation problem of iOMP which is stated in section III-A. Besides that, a detailed study of nOMP is introduced, which includes mathematical and simulation analysis. To evaluate the nOMP's performance precisely, two sets of atoms are selected, data-dependent atoms (learned atoms, non-orthogonal) and data-independent atoms (structured, quasi-orthogonal). Through an extensive experimentation (Experiments 1 & 2), by using standard images, we discussed the obtained results and validated the performance of the proposed method. Also, it was noted that, our approach outperforms iOMP significantly either by DDA or DIA.

Moreover, through several simulations with the USC-SIPI and Sentinel-1 dataset (Experiment 3), it was proved that, by merging some conventional methods such as BM3D, TVL1, SBATV and Bilateral methods to our approach, the overall performance is further improved. These results encourage us to make different hybrid techniques in the future.

REFERENCES

[1] A. M. Eskicioglu and P. S. Fisher, ''Image quality measures and their performance,'' *IEEE Trans. Commun.*, vol. 43, no. 12, pp. 2959–2965, Dec. 1995.

[2] P. Ndajah, H. Kikuchi, M. Yukawa, H. Watanabe, and S. Muramatsu, ''SSIM image quality metric for denoised images,'' in *Proc. 3rd WSEAS Int. Conf. Vis., Imag. Simul.*, Stevens Point, WI, USA, 2010, pp. 53–57.

[3] T. Pappas and R. Safranek, *Perceptual Criteria for Image Quality Evaluation*. New York, NY, USA: Academic, 2000, pp. 669–684.

[4] Z. Wang and A. C. Bovik, ''A universal image quality index,'' *IEEE Signal Process. Lett.*, vol. 9, no. 3, pp. 81–84, Aug. 2002.

[5] B. Goyal, A. Dogra, S. Agrawal, B. S. Sohi, and A. Sharma, ''Image denoising review: From classical to state-of-the-art approaches,'' *Inf. Fusion*, vol. 55, pp. 220–244, Mar. 2020. [Online]. Available: https://www.sciencedirect.com/science/article/pii/S1566253519301861

[6] H.-Y. Yang, X.-Y. Wang, P.-P. Niu, and Y.-C. Liu, ''Image denoising using nonsubsampled shearlet transform and twin support vector machines,'' *Neural Netw.*, vol. 57, pp. 152–165, Sep. 2014. [Online]. Available: https://www.sciencedirect.com/science/article/pii/S0893608014001439

[7] M. Elad and M. Aharon, ''Image denoising via sparse and redundant representations over learned dictionaries,'' *IEEE Trans. Image Process.*, vol. 15, no. 12, pp. 3736–3745, Dec. 2006.

[8] B. A. Olshausen and D. J. Field, ''Emergence of simple-cell receptive field properties by learning a sparse code for natural images,'' *Nature*, vol. 381, no. 6583, pp. 607–609, Jul. 1996.

[9] B. A. Olshausen and D. J. Field, ''Sparse coding with an overcomplete basis set: A strategy employed by V1,'' *Vis. Res.*, vol. 37, no. 23, pp. 3311–3325, 1997. [Online]. Available: http://www.sciencedirect.com/science/article/pii/S0042698997001697

[10] S. G. Mallat and Z. Zhang, ''Matching pursuits with time-frequency dictionaries,'' *IEEE Trans. Signal Process.*, vol. 41, no. 12, pp. 3397–3415, Dec. 1993.

[11] Y. Pati, R. Rezaiifar, and P. Krishnaprasad, ''Orthogonal matching pursuit: Recursive function approximation with applications to wavelet decomposition,'' in *Proc. Conf. Rec. 27th Asilomar Conf.*, Nov. 1993, pp. 40–44.

[12] S. Chen, S. A. Billings, and W. Luo, ''Orthogonal least squares methods and their application to non-linear system identification,'' *Int. J. Control*, vol. 50, no. 5, pp. 1873–1896, 1989, doi: 10.1080/00207178908953472.

[13] Z. Wang and A. C. Bovik, ''Mean squared error: Love it or leave it? A new look at signal fidelity measures,'' *IEEE Signal Process. Mag.*, vol. 26, no. 1, pp. 98–117, Jan. 2009.

[14] B. Efron, T. Hastie, I. Johnstone, and R. Tibshirani, "Least angle regression," *Ann. Statist.*, vol. 32, no. 2, pp. 407–451, 2004. [Online]. Available: http://www.jstor.org/stable/3448465
[15] L. Liu, L. Shao, F. Zheng, and X. Li, "Realistic action recognition via sparsely-constructed Gaussian processes," *Pattern Recognit.*, vol. 47, no. 12, pp. 3819–3827, Dec. 2014. [Online]. Available: https://www.sciencedirect.com/science/article/pii/S0031320314002659
[16] V. M. Patel and R. Chellappa, "Sparse representations, compressive sensing and dictionaries for pattern recognition," in *Proc. 1st Asian Conf. Pattern Recognit.*, 2011, pp. 325–329.
[17] Y. Yuan, X. Lu, and X. Li, "Learning hash functions using sparse reconstruction," in *Proc. Int. Conf. Internet Multimedia Comput. Service*, New York, NY, USA, 2014, pp. 14–18, doi: 10.1145/2632856.2632883.
[18] J. Wright, A. Y. Yang, A. Ganesh, S. S. Sastry, and Y. Ma, "Robust face recognition via sparse representation," *IEEE Trans. Pattern Anal. Mach. Intell.*, vol. 31, no. 2, pp. 210–227, Feb. 2009.
[19] D. L. Donoho, "For most large underdetermined systems of linear equations the minimal L1-norm solution is also the sparsest solution," *Commun. Pure Appl. Math.*, vol. 59, no. 6, pp. 797–829, 2006, doi: 10.1002/cpa.20132.
[20] E. J. Candés, J. K. Romberg, and T. Tao, "Stable signal recovery from incomplete and inaccurate measurements," *Commun. Pure Appl. Math.*, vol. 59, no. 8, pp. 1207–1223, May 2006, doi: 10.1002/cpa.20124.
[21] E. J. Candès and T. Tao, "Near-optimal signal recovery from random projections: Universal encoding strategies?" *IEEE Trans. Inf. Theory*, vol. 52, no. 12, pp. 5406–5425, Dec. 2006.
[22] Q. Lyu, Z. Lin, Y. She, and C. Zhang, "A comparison of typical ℓ_p minimization algorithms," *Neurocomputing*, vol. 119, pp. 413–424, Nov. 2013. [Online]. Available: https://www.sciencedirect.com/science/article/pii/S092523121300430X
[23] Z. Xu, X. Chang, F. Xu, and H. Zhang, "$\ell_{1/2}$ regularization: A thresholding representation theory and a fast solver," *IEEE Trans. Neural Netw. Learn. Syst.*, vol. 23, no. 7, pp. 1013–1027, May 2012.
[24] A. Y. Yang, S. S. Sastry, A. Ganesh, and Y. Ma, "Fast ℓ_1-minimization algorithms and an application in robust face recognition: A review," in *Proc. IEEE Int. Conf. Image Process.*, Jul. 2010, pp. 1849–1852.
[25] H. Li and F. Liu, "Image denoising via sparse and redundant representations over learned dictionaries in wavelet domain," in *Proc. 5th Int. Conf. Image Graph.*, Sep. 2009, pp. 754–758.
[26] K. Dabov, A. Foi, V. Katkovnik, and K. Egiazarian, "Image denoising by sparse 3-D transform-domain collaborative filtering," *IEEE Trans. Image Process.*, vol. 16, no. 8, pp. 2080–2095, Aug. 2007.
[27] J. Mairal, M. Elad, and G. Sapiro, "Sparse representation for color image restoration," *IEEE Trans. Image Process.*, vol. 17, no. 1, pp. 53–69, Jan. 2008.
[28] P. Chatterjee and P. Milanfar, "Clustering-based denoising with locally learned dictionaries," *IEEE Trans. Image Process.*, vol. 18, no. 7, pp. 1438–1451, Jul. 2009.
[29] A. Rehman, M. Rostami, Z. Wang, D. Brunet, and E. R. Vrscay, "SSIM-inspired image restoration using sparse representation," *EURASIP J. Adv. Signal Process.*, vol. 2012, no. 1, Dec. 2012.
[30] A. N. Omara, T. M. Salem, S. Elsanadily, and M. M. Elsherbini, "SSIM-based sparse image restoration," *J. King Saud Univ. Comput. Inf. Sci.*, Aug. 2021. [Online]. Available: https://www.sciencedirect.com/science/article/pii/S1319157821002056
[31] A. N. Omara, A. A. Hefnawy, and A. A. Zekry, "On sparse compression complexity of speech signals," *Indonesian J. Electr. Eng. Comput. Sci.*, vol. 17, no. 2, pp. 329–340, 2016.
[32] K. Dabov, A. Foi, V. Katkovnik, and K. Egiazarian, "Image denoising with block-matching and 3D filtering," in *Image Processing: Algorithms and Systems, Neural Networks, and Machine Learning*, vol. 6064, N. M. Nasrabadi, S. A. Rizvi, E. R. Dougherty, J. T. Astola, and K. O. Egiazarian, Eds. Bellingham, WA, USA: SPIE, 2006, pp. 354–365, doi: 10.1117/12.643267.
[33] Z. Zhi, B. Shi, and Y. Sun, "Primal-dual method to smoothing TV-based model for image denoising," *J. Algorithms Comput. Technol.*, vol. 10, no. 4, pp. 235–243, Dec. 2016, doi: 10.1177/1748301816656298.
[34] T. Goldstein and S. Osher, "The split Bregman method for L1-regularized problems," *SIAM J. Imag. Sci.*, vol. 2, no. 2, pp. 323–343, 2009, doi: 10.1137/080725891.
[35] C. Tomasi and R. Manduchi, "Bilateral filtering for gray and color images," in *Proc. 6th Int. Conf. Comput. Vis.*, Jan. 1998, pp. 839–846.
[36] K. Engan, S. O. Aase, and J. H. Husoy, "Method of optimal directions for frame design," in *Proc. IEEE Int. Conf. Acoust., Speech, Signal Process.*, vol. 5, Mar. 1999, pp. 2443–2446.
[37] *CVG-UGR Image Database*. Accessed: Jan. 10, 2021. [Online]. Available: http://decsai.ugr.es/cvg/dbimagenes/
[38] C. F. Lee, J. J. Shen, and K. T. Lin, "The study of steganographic algorithms based on pixel value difference," in *Advances in Intelligent Information Hiding and Multimedia Signal Processing* (Smart Innovation, Systems and Technologies), vol. 63, J. S. Pan, P. W. Tsai, and H. C. Huang, Eds. Cham, Switzerland: Springer, 2017, doi: 10.1007/978-3-319-50209-0_13.

A. N. OMARA received the B.Sc. degree in electronics and communications from the Shoubra Faculty of Engineering, Zagazig University, in 2003, and the M.Sc. and Ph.D. degrees in electronics and communications from the Faculty of Engineering, Ain Shams University, in 2011 and 2016, respectively. He has been with the Electronics Research Institute, since 2004. His current research interests include wireless networks and digital signal processing.

HESHAM FAROUK received the M.Sc. and Ph.D. degrees from the Electronics and Communications Department, Faculty of Engineering, Cairo University, in 1996 and 2001, respectively. He joined the Electronics Research Institute, Egypt, in 1993. His research interests include signal processing, mobile systems, neural networks, image compression, video processing, video compression, video indexing and retrieval, video on demand, pattern recognition, and machine vision. He has been a Professor, since 2019, and an Acting Manager with the Mobile, Social and Cloud Network Competence Center (MSCC), Ministry of Communication and Information Technology. He is the Vice President of the Mobile Task Force Group running under EITESAL. He is Cisco certified for CCNA and as an Instructor and certified from Improve Academy as an Innovation Guide.

SAYED A. MOHAMED received the B.Eng. degree in electronic engineering, in 1999, the M.Eng. degree in data analysis engineering, in 2010, and the Ph.D. degree in engineering science of industrial electronic and system engineering, in 2015, from the Faculty of Electronic Engineering, Menofia University. Since 2001, he has been with the Satellite Ground Receiving Station and Data Processing, National Authority for Remote Sensing and Space Sciences, Cairo, Egypt. He has over 20 years of experience in the field of receiving and image processing of remotely sensed data. He has authored or coauthored more scientific publications, including journals and conference proceedings. His research interests include applications of artificial intelligence tools and neural networks to digital image processing in the field of computer vision, remote sensing, and geographical information data.